Controlled Aggregation of Magnetic Ions in a Semiconductor: An Experimental Demonstration

A. Bonanni,[1,*] A. Navarro-Quezada,[1] Tian Li,[1] M. Wegscheider,[1] Z. Matěj,[2] V. Holý,[2] R. T. Lechner,[1] G. Bauer,[1] M. Rovezzi,[3] F. D'Acapito,[3] M. Kiecana,[4] M. Sawicki,[4] and T. Dietl[4,5]

[1]*Institute for Semiconductor and Solid State Physics, Johannes Kepler University, A-4040, Linz, Austria*
[2]*Department of Condensed Matter Physics, Charles University, CZ-121 16 Prague, Czech Republic*
[3]*INFM-OGG, c/o GILDA CRG-ESRF, Boîte Postale 220, F-38043 Grenoble, France*
[4]*Institute of Physics, Polish Academy of Sciences, PL-02-668 Warszawa, Poland*
[5]*Institute of Theoretical Physics, University of Warsaw, PL-00-681 Warszawa, Poland*

(Received 23 April 2008; published 25 September 2008)

The control on the distribution of magnetic ions into a semiconducting host is crucial for the functionality of magnetically doped semiconductors. Through a structural analysis at the nanoscale, we give experimental evidence that the aggregation of Fe ions in (Ga,Fe)N and consequently the magnetic response of the material are affected by the growth rate and doping with shallow impurities.

DOI: 10.1103/PhysRevLett.101.135502 PACS numbers: 61.46.Hk, 64.75.Qr, 75.50.Pp, 81.15.Gh

There is an increasing amount of evidence that, owing to specific features of magnetic impurities in wide band-gap semiconductors and oxides, the epitaxial growth of these systems can result in the self-organized aggregation of magnetically robust nanocrystals embedded in the host paramagnetic matrix [1–3]. With no doubt this finding holds enormous potential for the fabrication of a range of multifunctional nanosystems relevant to spintronics, nanoelectronics, photonics, and plasmonics [2,4]. However, it has also been realized [5] that enduring difficulties in the experimental resolution and identification of the embedded nanostructures hamper the progress in the control of the mechanisms accounting for relevant and hitherto unexplored nanoassembly processes.

In this Letter, by exploiting state-of-the-art nanocharacterization tools, we show how growth conditions and codeposition with shallow donors or acceptors affect the distribution of the magnetic ions in (Ga,Fe)N deposited by metalorganic vapor phase epitaxy (MOVPE), emphasizing conclusions that are pertinent to the whole class of wide band-gap diluted magnetic semiconductors (DMS) and diluted magnetic oxides (DMO) extensively studied over the past eight years [1,6,7]. In particular, we identify different ways by which transition metal (TM) impurities can incorporate into the host semiconducting lattice and we link the structure investigated at the nanoscale to the macroscopic magnetic properties. Our findings show that Fermi-level tuning by doping with shallow impurities is instrumental in controlling the magnetic ion aggregation. This provides experimental support to recent theoretical suggestions [8] and it demonstrates that the Fermi-level engineering documented so far for iodine and nitrogen doped (Zn,Cr)Te [5] operates also in the case of III-V DMS.

All studied epilayers have been fabricated by MOVPE on *c*-plane sapphire substrates employing the growth protocols and the *in situ* and *ex situ* characterization methods we reported previously for (Ga,Fe)N [9] and GaN:Mg [10] and that we apply now to produce (Ga,Fe)N and (Ga,Fe)N:Si,Mg layers. The total Fe concentration in these samples varies from 4×10^{19} to 3×10^{20} cm^{-3} for the Fe-precursor (Cp_2Fe) flow rate ranging from 50 to 300 sccm [9,11]. The Mg concentration is found to be in the range $2–3 \times 10^{19}$ cm^{-3} [10] and the Si content is estimated to be 1×10^{19} cm^{-3}. The growth rate during deposition is regulated by the Ga-precursor (TMGa) flow rate and attains 0.3 nm/s for 12 sccm of TMGa flow. The difference between the magnetization values measured by SQUID magnetometery up to 5 T at 1.8 and 5 K is employed to determine the concentration $n_{Fe^{3+}}$ of paramagnetic Fe^{3+} ions in the layers, which agrees within a factor of 2 with the value of $n_{Fe^{3+}}$ obtained from electron spin resonance measurements [9]. Low-field and low-temperature hysteresis loops allow us to evaluate the concentration of Fe contributing to the ferromagnetic signatures, n_{ferro}, which we

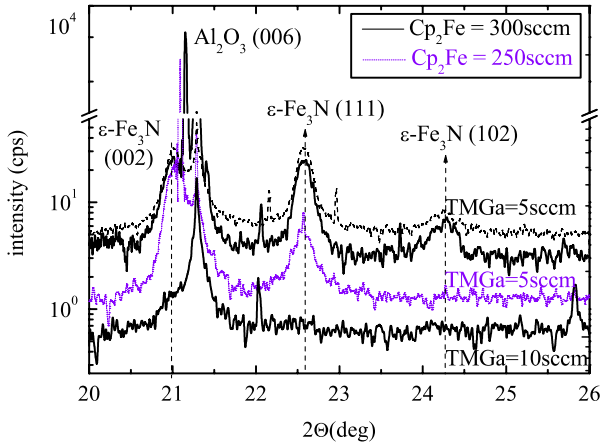

FIG. 1 (color online). Synchrotron radiation powder XRD spectra versus Fe content and growth rate for (Ga,Fe)N, as indicated. The two uppermost traces are generated by the same sample, but measured at different rotation angles.

determine assuming a magnetic moment of $2\mu_B$ per Fe ion [11].

In addition to TEM and energy dispersive spectroscopy [9], we have performed and present here Fourier filtering of the TEM images [12] for strain analysis [13], reconstructed by using the 002 spatial frequency. Powder x-ray diffraction (XRD) measurements have been carried out at the beam line ID31 of the ESRF (Grenoble, France) using a photon energy of 15.5 keV. The x-ray data correspond to the diffracted intensities in reciprocal space along the sample surface normals, collected using a secondary crystal monochromator in front of the detector; thus, the GaK_α fluorescence is suppressed. We have acquired symmetric $\omega/2\Theta$ scans with scattering angles 2Θ up to 150° and found that the most intense peaks appear in the 2Θ range up to 25°. As at the powder diffraction beam line the sample tilt cannot be adjusted, neither the position nor the intensity of the substrate peaks may be compared for different scans (see the difference between the two upmost curves in Fig. 1). In contrast, the peaks for small nanocrystals are broad, and thus virtually insensitive to the sample tilt.

It has already been established that once the solubility limit of Fe in GaN at the given growth conditions is exceeded, the ferromagnetic response of (Ga,Fe)N increases with the Cp_2Fe flow rate [9]. In Fig. 1 we report the XRD scans for (Ga,Fe)N samples with different Fe content above its solubility limit. For the samples deposited at the low growth rate (TMGa at 5 sccm), in contrast to laboratory high-resolution XRD which does not evidence any phase separation in (Ga,Fe)N [9], the high intensity available at the synchrotron beam line allows one to reveal the presence of new diffraction peaks identified as the (002) and (111) of the phase ε-Fe_3N [hexagonal siderazot structure, space group no. 182 ($P6_322$), lattice parameters $a = 0.4698$ nm and $c = 0.4379$ nm, Curie temperature $T_C = 575$ K, and magnetic moment per Fe ion $m = 2\mu_B$ [14]]. This assignment is consistent with the crystallographic characteristics of the Fe-rich secondary phases as put on view by TEM images and summarized in Fig. 2. The height of the ε-Fe_3N-related diffraction maxima is enhanced with increasing the flow rate of Cp_2Fe; however, no significant dependence of their FWHM is observed upon varying the nominal content of magnetic ions. This implies that the mean size of the precipitates does not substantially vary with increasing the nominal Fe content, whereas their density is enhanced, as confirmed by TEM [9]. We are, thus, led to the conclusion that the precipitation occurs by a nucleation mechanism in which only nanocrystals with a critical size can form. We use the FWHM of all diffraction maxima of ε-Fe_3N for an estimate of the mean size of the precipitates, and by employing the Williamson-Hall plot method [15] we obtain an average value for the nanocrystals diameter of 15 ± 5 nm.

Our studies for various growth rates demonstrate that the nanocrystal nucleation is limited by a kinetic barrier for the surface Fe diffusion. As shown in Fig. 1 the diffraction peaks originating from the Fe-rich nanocrystals appear only in the slow growth-rate regime (samples grown with TMGa at 5 sccm) and are quenched at higher growth rates, as evidenced by the lowest XRD trace in Fig. 1, obtained for the layer deposited at 10 sccm TMGa. Figure 3(b) gives the normalized number of Fe ions contributing to the ferromagnetic signatures n_{ferro} as a function of the TMGa precursor flow rate (i.e., the growth rate), and its decrease with increasing flow rate agrees with the XRD data, giving evidence of a reduced contribution of Fe-rich magnetic nanocrystals at higher growth rates. It is interesting to note that this is in contrast to the case of (Ti, Cr)O_2, where faster growth rates lead to a stronger ferromagnetic response correlated with the density of extended defects such as grain boundaries [16]. At intermediate values of growth rate (e.g., TMGa at 10 sccm) and a Fe-precursor flow rate of 300 sccm, where with synchrotron XRD the

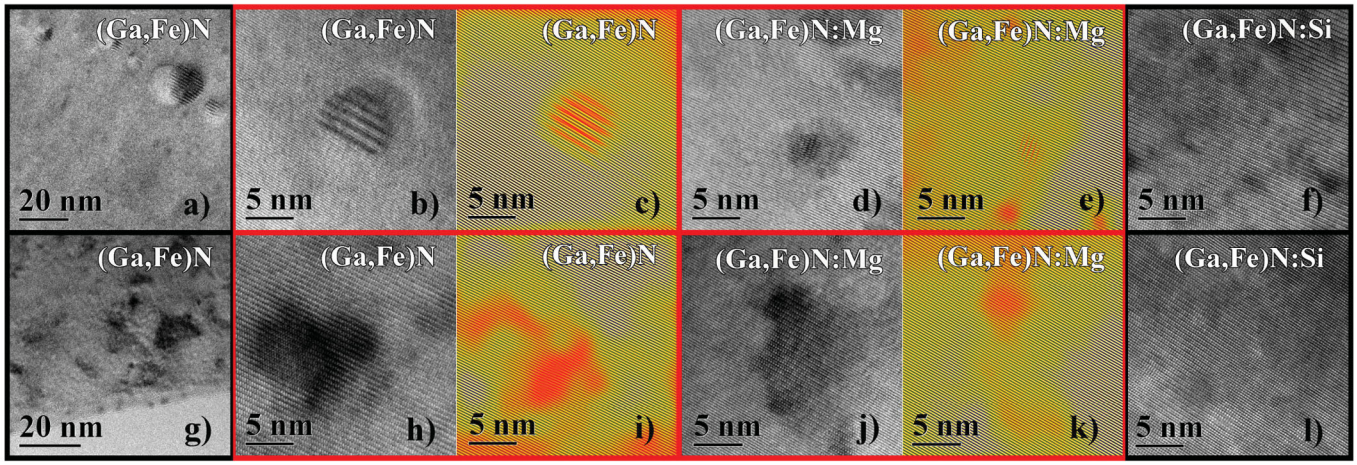

FIG. 2 (color). Bright-field images (a),(g), TEM with mass contrast (b),(d),(f),(h),(j),(l), and Fourier filtered images with strain mapping (c),(e),(i),(k) of (Ga,Fe)N revealing the presence of Fe_3N precipitates (a)–(e), spinodal decomposition (g)–(k), and the effect of codeposition of either Si (f),(l) or Mg (d),(e),(j),(k) preventing the formation of the Fe-rich regions.

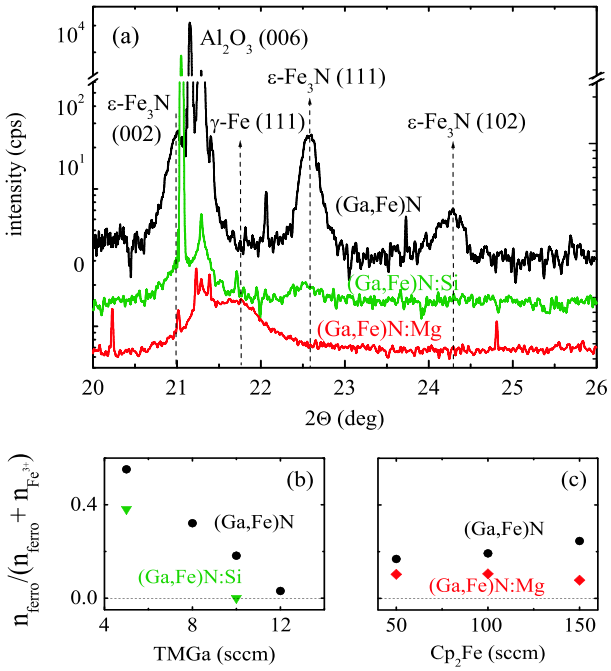

FIG. 3 (color online). Effect of Si and Mg doping on the synchrotron radiation powder XRD spectra (a) and on the normalized number of Fe ions contributing to the ferromagnetic signatures in (Ga,Fe)N versus TMGa flow rate, i.e., growth rate, (b) and versus Cp_2Fe flow rate (c).

onset of second phases is not detected, ferromagnetic signatures are still clearly seen by SQUID up to a blocking temperature T_B typically over 300 K. These puzzling observations are elucidated by the TEM images with mass contrast and strain mapping, shown in Figs. 2(g)–2(l), that put into evidence the presence of spinodal decomposition into nanoscale regions with high Fe content embedded in the Fe-poor matrix without any crystallographic phase separation. This effect is being referred to as spinodal decomposition independently of the microscopic mechanisms involved. This appears as a generic property of a number of DMS and DMO, in which no precipitates are detected, but ferromagnetic features persist up to high temperatures [7]. While the exact content of the magnetic component has not yet been evaluated, the stability of T_C (in contrast to T_B and n_{ferro}) may indicate that the commensurate nanocrystals have a defined chemical composition.

Remarkably, our TEM, XRD, and SQUID data reveal that the aggregation of Fe ions can be diminished or even prevented by doping with either Si donors or Mg acceptors. Figure 2 presents TEM data for the two relevant initial regimes, namely, (Ga,Fe)N with embedded Fe-rich nanocrystals [Figs. 2(a)–2(f)] evidenced by moiré fringes contrast and (Ga,Fe)N showing spinodal decomposition [Figs. 2(g)–2(l)] generating mass contrast and lattice distortion, as proved by the filtered images [Figs. 2(i)–2(k)]. From Figs. 2(d)–2(f) and 2(j)–2(l) the reduced aggregation of Fe-rich regions as a consequence of codeposition with Si and Mg, respectively, is evident. This effect is further corroborated by the XRD results given in Fig. 3. In both cases, the shallow impurities are found to hamper efficiently the precipitate aggregation, so that the diffraction peaks corresponding to ε-Fe_3N are suppressed in the case of codoped samples. We point out that the XRD curve from the Mg-doped sample exhibits also a broad maximum identified as the (111) diffraction from pure γ-Fe (austenite). This finding is supported by our TEM observations, revealing in the considered sample the presence of a few-nm thick Fe inclusions at the surface. The suppression of the ferromagnetic contribution in the doped samples is further validated by the reduced number of average Fe ions adding to the ferromagnetic response in both Si- and Mg-doped (Ga,Fe)N layers. In Fig. 3(b), the quenching of the ferromagnetic contribution by Si doping is equally observed in samples deposited at a low growth rate (5 sccm TMGa, i.e., presenting Fe-rich nanocrystals when not Si or Mg doped) and at intermediate growth rate (10 sccm TMGa, i.e., showing when not Si- or Mg-doped spinodal decomposition). The change in the normalized n_{ferro} upon codeposition with acceptors is presented in Fig. 3(c) as a function of the nominal Fe content in the low magnetic ion doping regime (Cp_2Fe at 50–150 sccm).

In order to explain these key findings, we note that except for Mn in II-VI compounds [5], owing to the presence of the open d shells in the vicinity of the Fermi level, the nearest neighbor pair of TMs in semiconductors shows a large binding energy which promotes the magnetic ion aggregation. This effect is well documented in the bulk [2,5,17], but owing to a relatively weak sensitivity of the d-level positions to the chemical environment [6], it should persist for Fe ions at the surface. However, if carriers introduced by doping can be trapped by these ions, the pair binding energy will be altered, usually reduced by the corresponding Coulomb repulsion [5,8].

While the presence of the midgap electron trap, i.e., the Fe^{+3}/Fe^{+2} state, is well established in GaN [6], the level Fe^{+3}/Fe^{+4} is expected to reside rather in the valence band [6]. However, it has been recently suggested that the potential introduced by the Fe^{+3} ion is strong enough in GaN to bind a hole [18]. Furthermore, it appears that at high values of the Fe flow rate the carrier trapping by the Fe ions may not be complete, presumably because of a gradient in the Fe distribution along the growth direction [9]. Thus, the effect of codeposition on the Fe charge state has to be experimentally assessed. We have found that the Fe K edge probed by the x-ray absorption spectroscopy (XAS) shifts under Si doping from a position expected for the Fe^{3+} oxidation state towards that specific to the Fe^{+2} configuration [19]. The $Fe^{3+} \rightarrow Fe^{2+}$ transmutation upon the Si doping is also documented by a decrease in the photoluminescence intensity corresponding to the Fe^{3+} internal transitions [9]. By contrast, this intensity becomes stronger in the films containing Mg [9], which can be explained by an admixture of the p-type wave function brought by the trapped hole.

In view of these findings and since the concentrations of Si and Mg are comparable to that of n_{ferro} in our samples, the obstructive effect of Si or Mg doping on the nanocrystal formation and, thus, on the ferromagnetic response, can be elucidated in terms of the corresponding alternation of the Fe valence. Significantly, in view of our results, the previously observed effect of doping on ferromagnetism in (Ga,Mn)N, and assigned to the dependence of the double exchange mechanisms of the spin-spin coupling on the position of the Fermi level with respect to the center of the d band [20], has to be reconsidered. Furthermore, since with the experimental resolution of $5 \times 10^{16} \mu_B/\mathrm{cm}^3$ we do not observe any spontaneous magnetization in GaN, GaN:Si, and GaN:Mg down to 5 K, we conclude that the recently invoked vacancy-related ferromagnetism of GaN [21] is not present in our samples.

In summary, by combining TEM and synchrotron XRD with SQUID we have identified three distinct ways by which Fe incorporates into the GaN lattice: (i) substitutional Fe^{3+} diluted ions accounting for the paramagnetic response [9], (ii) Fe-rich (Ga,Fe)N wurtzite nanocrystals commensurate with and stabilized by the GaN host lattice, and (iii) hexagonal ϵ-Fe_3N precipitates. The formation of nanocrystals containing a large density of the magnetic constituent elucidates the origin of the ferromagnetic features persisting up to above room temperature. Importantly, the doping with either Si or Mg hampers the nanocrystal assembling. This demonstrates that the charging of the magnetic ions, $Fe^{3+} \rightarrow Fe^{2+}$ and $Fe^{3+} \rightarrow Fe^{3+} + h$, respectively, inhibits the Fe aggregation and explains the sensitivity of the ferromagnetic response to doping with shallow donors or acceptors. Furthermore, the influence of the growth rate on the nanocrystal formation indicates that the Fe aggregation occurs at the growth surface. Since, quite generally, the binding energy of TM pairs depends on the valency of the open d shells, there are grounds to suppose that the Fermi-level engineering evoked here for (Ga,Fe)N:Si,Mg can serve to control the magnetic ion aggregation in a number of semiconductors and oxides, providing a way to the self-organized fabrication of multicomponent systems with tailored magnetic, magneto-optical, and magnetotransport properties at the nanoscale.

This work has been supported by the Austrian Fonds zur Förderung der wissenschaftlichen Forschung (P18942, P20065, and N107-NAN), by the Czech Grant Agency (202/06/0025) and Ministry of Education (MSM 0021620834), and by the EC (NANOSPIN, FP6-2002-IST-015728; SPINTRA, ERAS-CT-2003-980409). We acknowledge the assistance of the ID31 staff at the ESRF.

*alberta.bonanni@jku.at

[1] A. Bonanni, Semicond. Sci. Technol. **22**, R41 (2007), and references therein.
[2] H. Katayama-Yoshida, K. Sato, T. Fukushima, M. Toyoda, H. Kizaki, V. A. Dinh, and P. H. Dederichs, Phys. Status Solidi A **204**, 15 (2007).
[3] M. Jamet, A. Barski, T. Devillers, V. Poydenot, R. Dujardin, P. Bayle-Guillmaud, J. Rotheman, E. Bellet-Amalric, A. Marty, J. Cibert, R. Mattana, and S. Tatarenko, Nature Mater. **5**, 653 (2006).
[4] T. Dietl, J. Appl. Phys. **103**, 07D111 (2008).
[5] S. Kuroda, N. Nishizawa, M. Mitome, Y. Bando, K. Osuch, and T. Dietl, Nature Mater. **6**, 440 (2007).
[6] E. Malguth, A. Hoffmann, and M. R. Phillips, Phys. Status Solidi B **245**, 455 (2008), and references therein.
[7] C. Liu, F. Yun, and H. Morkoç, J. Mater. Sci.: Mater. Electron. **16**, 555 (2005); S. J. Pearton, C. R. Abernathy, M. E. Overberg, G. T. Thaler, D. P. Norton, N. Theodoropoulou, A. F. Hebard, Y. D. Park, F. Ren, J. Kim, and L. A. Boatner, J. Appl. Phys. **93**, 1 (2003); S. A. Chambers, T. C. Droubay, C. M. Wanga, K. M. Rosso, S. M. Heald, D. Schwartz, K. R. Kittilstved, and D. Gamelin, Mater. Today **9**, 28 (2006).
[8] T. Dietl, Nature Mater. **5**, 673 (2006); L.-H. Ye and A. J. Freeman, Phys. Rev. B **73**, 081304(R) (2006).
[9] A. Bonanni, M. Kiecana, C. Simbrunner, T. Li, M. Sawicki, M. Wegscheider, M. Quast, H. Przybylińska, A. Navarro-Quezada, R. Jakieła, A. Wolos, W. Jantsch, and T. Dietl, Phys. Rev. B **75**, 125210 (2007).
[10] C. Simbrunner, M. Wegscheider, M. Quast, Tian Li, A. Navarro-Quezada, H. Sitter, A. Bonanni, and R. Jakiela, Appl. Phys. Lett. **90**, 142108 (2007).
[11] See EPAPS Document No. E-PRLTAO-101-053840 for a table summarizing Fe concentrations in the studied films. For more information on EPAPS, see http://www.aip.org/pubservs/epaps.html.
[12] X. R. Huang, J. Baj, M. Dudley, B. Wagner, R. F. Davis, and Y. Zhu, Phys. Rev. Lett. **95**, 086101 (2005).
[13] D. Litvinov, D. Gerthsen, A. Rosenauer, M. Schowalter, T. Passow, P. Feinaugle, and M. Hetterich, Phys. Rev. B **74**, 165306 (2006).
[14] A. Leineweber, H. Jacobs, F. Höning, H. Luekenb, H. Schilderc, and W. Kockelmannd, J. Alloys Compd. **288**, 79 (1999).
[15] B. E. Warren, *X-Ray Diffraction* (Dover New York, 1990).
[16] T. C. Kaspar, T. Droubay, V. Shutthanandan, S. M. Heald, C. M. Wang, D. E. McCready, S. Thevuthasan, J. D. Bryan, D. R. Gamelin, A. J. Kellock, M. F. Toney, X. Hong, C. H. Ahn, and S. A. Chambers, Phys. Rev. B **73**, 155327 (2006).
[17] M. van Schilfgaarde and O. N. Mryasov, Phys. Rev. B **63**, 233205 (2001).
[18] T. Dietl, Phys. Rev. B **77**, 085208 (2008).
[19] See EPAPS Document No. E-PRLTAO-101-053840 for the XAS results. For more information on EPAPS, see http://www.aip.org/pubservs/epaps.html.
[20] M. J. Reed, F. E. Arkun, E. A. Berkman, N. A. Elmasry, J. Zavada, M. O. Luen, M. L. Reed, and S. M. Bedair, Appl. Phys. Lett. **86**, 102504 (2005); M. H. Kane, M. Strassburg, E. W. Fenwick, A. Asghar, A. M. Payne, S. Gupta, Q. Song, Z. J. Zhang, N. Dietz, C. J. Summers, and I. T. Ferguson, J. Cryst. Growth **287**, 591 (2006).
[21] P. Dev, Y. Xue, and P. Zhang, Phys. Rev. Lett. **100**, 117204 (2008).